Addendum to the NA43 p

CERN/SPSC 90-31
SPSC/P234 Add. 3
12 October 1990

Investigations of the coherent hard photon yields from (50-300) GeV/c electrons/positrons in the strong crystalline fields of diamond, silicon and germanium crystals

R. Medenwaldt, S.P. Møller*, A.H. Sørensen,
E. Uggerhøj**, T. Worm,
Institute for Synchrotron Radiation,
Aarhus University,
DK-8000 Aarhus C,
Denmark.

M. Hage-Ali, P. Siffert, J. Stoquert,
Centre de Recherches Nucleaires,
F-67037 Strasbourg Cedex
France.

P. Sona,
Dipartimento di Fisica
Universita di Firenze, and
Istituto Nazionale di Fisica Nucleaire
I-50125 Florence, Italy.

S.H. Connell, J.P.F. Sellschop,
University of Witwatersrand,
P.O. Wits
2050 Johannesburg,
R.S.A.

R.O. Avakian, H.I. Avetisian, S.P. Taroian,
Yerevan Physics Institute,
Yerevan 375036, Armenia
USSR.

*) contactman
**) spokesman

SUMMARY

The aim of this experiment is to measure for the first time the influence of strong fields on emission of coherent radiation, when multi-hundred GeV electrons/positrons penetrate single crystals near axial/planar directions. The targets will be diamond, Si, Ge, and W crystals.

When multi-GeV electrons and positrons penetrate single crystals near axial/planar directions dramatic effects appear. The large gamma factors (10^5-10^6) enhance the electric fields along axes/planes to overcritical values within the electron restframe. Overcritical in this context means that perturbation theory (used hitherto) is no longer applicable, but a full description of QED in strong fields has to be used. Bremsstrahlung becomes a highly non-perturbative process resulting in a much enhanced cross section. Originally NA-33 found a peak in the photon spectra from 150 GeV electrons penetrating Ge-crystals. In the literature different suggestions for processes leading to this peak is found, i.e. "new" physics, radiation cooling, multiphotons etc. Along axial/planar directions these effects were investigated in detail (figs. 3-10) by NA-43 and surprising effects were found. 150 GeV axially channeled electrons radiate 80% of the total energy E_0 in 1 mm Ge - 20 times more that in amorphous material. The peak in the photon spectra around (0.8-0.9) $\times E_0$ is a multiphoton effect and found both in Si and Ge, but not for thin Si-crystal and not for incident angles larger than $\sim 0.5 \times$ the channeling angle ψ_1. The influence of strong fields on shower formation was also measured by NA-43 along axial directions. Radiation lengths are (10-50) times shorte than Bethe-Heitler values. The angular dependence is in agreement with the critical angle $\theta_0 = U_0/mc^2 \sim 0.5$ mrad calculated by Baier et al. for strong field effects.

For coherent bremsstrahlung the theory predicts (figs. 12, 13) dramatic enhancements (~ 100 in diamond) over B-H yields for incident angles around θ_0. The peaks are single photons with energies of (0.5-0.9) times the particle energy E_0. For W such effects were already seen by NA-43 (fig. 10). As compared to results from Born approximation the predictions by Baier et al. are (5-10) times larger. The applications of such high energy, high intensity, and nearly monoenergetic photon beams in particle physics is obvious and has been discussed in different papers (refs. 28-31).

For investigations of the predicted strong field effects the experimental setup used by NA-43 (fig. 14) in the H2 beam of the North Hall is unique. The driftchambers 50 m apart give angular resolutions of ~ 2 μrad. The crystal mounting and goniometer surrounded by a temperature regulated hut gave very accurate and reproducable angle settings and long-term stability. Diamond, Si, Ge, an d W-crystals are available.

Beam and beam time.

For the investigation is needed electrons/positrons with energies up to 200 GeV/c or more. Angular divergence ~ 50 μrad and intensity 10^2-10^5 particles/sec., beam diameter less than 10 mm. These reguirements are fulfilled by the H2 beam in the North Hall. For installation, setting up, and data taking 2 weeks of beam time are needed. The experimental equipment is the same as last time.

I PHYSICS BACKGROUND

In this chapter is given a short review on the physics around radiation emission in single crystals. Special regard is given to the strong field effects experienced by ultrarelativistic particles traversing single crystals in near axial directions.

1. BREMSSTRAHLUNG

The radiation emitted by a charged particle penetrating an atomic field is known as incoherent bremsstrahlung IBS. At high velocities, the emission process requires a quantum-mechanical description and, in the Born limit $Z\alpha << 1$, the cross section for photon emission at energy $\hbar\omega$ upon relativistic electron/positron impact at total energy E reads approximately[1]

$$\frac{d\sigma}{d\hbar\omega} = \frac{16}{3} Z^2 \alpha r_e^2 \frac{1}{\hbar\omega} \left(1 - \frac{\hbar\omega}{E} + \frac{3}{4} \left(\frac{\hbar\omega}{E} \right)^2 \right) \ln\left(183 Z^{-1/3}\right) \tag{1}$$

Here $r_e = e^2/mc^2 = \alpha^2 a_0$ denotes the classical electron radius, α is the finestructure constant, and Z the target atomic number. The result (1) holds when the atomic (Thomas-Fermi) screening is "complete" which requires the Lorenz factor $\gamma >> 1$. Otherwise, the argument of the logarithm is changed. At moderate values of γ, Equation (1) still holds for soft photons, $\hbar\omega/E << 1$. As it stands, the expression (1), which we shall call the Bethe-Heitler cross section, covers the radiation emitted as a result of scattering in the screened field of the atomic nucleus. Furthermore, radiation may be emitted as a result of direct scattering on target electrons. In order of magnitude this leads to an extra contribution to the cross section of $1/Z$ times the nuclear one, (1).

In addition to the dependence on photon energy, which is essentially as $1/\hbar\omega$ according to Equation (1), also the dependence of the bremsstrahlung-emission probability on photon-emission angle is of interest: At high energies, photons are emitted in a narrow cone of opening angle $\sim 1/\gamma$ around the initial direction of motion of the projectile.

For a high-energy electron or positron ($\geq$1 GeV for most materials), the major cause of slowing down is by far emission of bremsstrahlung. It is convenient for later use to introduce the so-called radiation length l_r, which is defined as the penetration depth over which such a projectile on an average loses all but a fraction $1/e$ of its initial energy. From Equation (1) we find that the total stopping cross section $S \equiv \int \hbar\omega \, d\sigma$ is simply proportional to the primary energy, $S = \sigma_0 E$, where σ_0 is energy independent, and the radiation length therefore is simply given as $l_r = 1/n\sigma_0$, that is, for a homogeneous (amorphous) medium, we have

$$l_r^{-1} = 4Z^2\alpha n r_e^2 \ln\left(183Z^{-1/3}\right). \qquad (2)$$

Here n is the target atomic density.

Corrections to (2) are of the same relative order as to (1), namely l/Z and $(\alpha Z)^2$. Furthermore, for very light targets, Z≤5, screening should be described more accurately than by the statistical Thomas-Fermi model. Table I lists examples of radiation lengths for materials of interest in the present context.

TABLE I

Radiation lengths (in cm) for various materials. The values tabulated in the first column correspond to the expression (2), wheres those in the last column are the "exact" ones.

Material	**l_r (Equation (2))**	**l_r (exact)**
C (graphite)	22.9	18.8
C (diamond)	14.8	12.2
Si	10.2	9.36
Ge	2.35	2.30
W	0.33	0.35

2. COHERENT BREMSSTRAHLUNG

When an electron or a positron penetrates a single crystal in a direction close to a major crystallographic axial or planar direction, it has a fair chance to scatter coherently on many target atoms along its way. Channeling, of course, is an example of this. The coherence in scattering is carried on to the radiation emission and, consequently, the emission in a single crystal may greatly exceed the bremsstrahlung emission in a similarly dense but amorphous medium composed of the same type of atoms. We shall study the radiation emission during channeling in the sections following below. In this section, however, let us consider the emission process in the limit where the projectile interaction both with the radiation field and with the crystal atoms may be treated in the Born approximation. According to custom, we call this the case of "coherent bremsstrahlung"[2, 3] (CBS).

In the perturbation limit, the bremsstrahlung-emission probability is proportional to the square of a second-order matrix element which, in turn, is composed as a sum of terms, each proportional to the product of two first-order matrix elements, one for the interaction with the radiation field and one for the scattering in the atomic field[1]. Since the projectile states are plane waves, we have immediately

$$d\sigma \propto \left| \int V(r) e^{i\vec{q}\vec{r}}\, d^3\vec{r} \right|^2 \qquad (3)$$

where V is the atomic potential and $\hbar\vec{q}$ is the recoil momentum of the atomic nucleus. In case we consider bremsstrahlung production upon incidence on a total of N atoms, the above potential V needs to be replaced by the total interaction potential,

$$V \rightarrow \sum_n V(\vec{r} - \vec{r}_n). \tag{4}$$

Here $\vec{r}_n$ denotes the position of the n' th atom. In applying the expression (4), we neglect changes appearing in the potential as a result of rearrangements of the outermost parts of the atomic electron cloud wich results from mutual atom-atom interactions. This is justified since the target electrons essentially only enter in the screening of the nuclear charge. Substituting the sum (4) for the interaction potential into Equation (3), we get the following relation between the differential cross sections for photon production at energy $\hbar\omega$ on an isolated atom and on the group of N atoms,

$$\left.\frac{d\sigma}{d\hbar\omega d^3\vec{q}}\right|_{N\text{ atoms}} = \left.\frac{d\sigma}{d\hbar\omega d^3\vec{q}}\right|_{\text{single atom}} \left|\sum_n e^{i\vec{q}\vec{r}_n}\right|^2 . \tag{5}$$

For an amorphous medium, the last factor yields just N. On the other hand, for a perfect static single crystal, we find in the limit $N \rightarrow \infty$

$$\left|\sum_n e^{i\vec{q}\vec{r}_n}\right|^2 = N\frac{(2\pi)^3}{N_0\Delta} |S(\vec{g})|^2 \sum_{\vec{g}} \delta(\vec{q}-\vec{g}). \tag{6}$$

Here $\vec{g}$ denotes a reciprocal lattice vector, $S(\vec{g})$ the structure factor, and N_0 is the number of atoms contained in a unit cell which has the volume Δ. This result is well known from diffraction theory.

The interference structure suggested by Equations (5-6) is softened some-what as a result of thermal vibrations. Inclusion of phonon excitation in the description outlined, leads to a replacement of the interference factor in Equation (5) by its thermal average which reads[3]

$$\left\langle\left|\sum_n e^{i\vec{q}\vec{r}_n}\right|^2\right\rangle_T = N[1 - \exp(-q^2\rho_1^2)] + \exp(-q^2\rho_1^2)\left|\sum_n e^{i\vec{q}\vec{r}_{n0}}\right|^2. \tag{7}$$

Here $\vec{r}_{n0}$ denotes the equilibrium or static lattice sites, while ρ_1 is the one-dimensional vibrational amplitude $(2\rho_1^2 = \rho^2)$. Due to thermal scattering, the interference factor is reduced by a Debye-Waller factor, as revealed by the second term on the right-hand side of Equation (7). We call the part of the radiation corresponding to this term the *interference* or *coherent* part. In addition an *incoherent* or *amorphous* part exists, corresponding to the first term on the right-hand side of (7). Except for a slight reduction due to the square-bracket factor (one minus a Debye-Waller factor), this part is identical to Bethe-Heitler bremsstrahlung for an amorphous medium.

Explicit expressions for the amorphous and the interference cross section may be found in many texts[2,3].

Figure 1 shows examples of coherent-bremsstrahlung spectra computed for high-energy electrons incident near the <110> axis in a germanium single crystal. The polar angle of incidence to the axis is fixed, but two different azimuthal angles have been chosen. Both for incidence in a plane and for incidence at a "random" azimuthal angle (far from major planes), there is a strong enhancement of the radiation yield as compared to the amorphous yield, Equation (1). In addition, for incidence in a plane, strong interference peaks show up due to periodic passing of different axes. The spectra correspond to integration over all emission angles. If a collimation is performed in, say, the forward direction, the smooth fall-off of each spike on the low-energy side would disappear, and narrow peaks, sharp on both sides, would remain at the positions of the maxima.

3. CHANNELING RADIATION

If the direction of incidence is nearly parallel to axial or planar directions, the projectile motion becomes governed by the lattice continuum potential obtained by smearing the atomic charges along axes or planes. The resulting strong steering effect is known as channeling[4,5,6].

The basic quantity determining the incident angular condition under which channeling effects occur is for axis the critical angle ψ_1

$$\psi_1 = \sqrt{\frac{4Z_1Z_2e^2}{pvd}} \tag{8}$$

where p and v is the (relativistic) momentum and velocity respectively, d is the lattice constant and Z_1 and Z_2 the projectile and target nuclear charge. The corresponding planar critical angle ψ_p is

$$\psi_p = \sqrt{\frac{4Z_1Z_2e^2Nd_pCa}{pv}} \tag{9}$$

where C is a constant $\sim \sqrt{3}$ and $a = a_0\, Z_2^{-1/3}$ is a screening length, a_0 being the Bohr radius.

The channeling motion also gives rise to coherence effects, and the ensuing radiation is called channeling radiation (ChR)[7, 8, 9]. The structure of ChR is strongly connected to the form of the trapping potentials but is not (as is CBS) directly connected to the lattice parameters. In the channeling picture, positrons are pushed away from atomic axes and planes, whereas electrons are focused around the nuclei. The two types of particles therefore "see" different potentials, and their ChR spectra will be different in shape, which is not the case for CBS.

In a quantal description of channeling Lindhard[10] showed that the number of quantum states ν corresponding to a transverse bound motion is proportional to the Lorenz factor γ. So for electrons/positrons in the GeV region the number of channeling states become large and the level spacing reduce correspondingly. As a result essentially continous transitions down through the dense spectra of states becomes possible. Hereby ChR appears as a classical emission process.

The computation of the radiation spectra for channeled GeV electrons or positrons follows standard recipes of classical electrodynamics. Having determined the trajectory $\vec{r}(t)$ of a particle according to the equations of motion, the energy radiated per unit frequency and unit solid angle may be found as[11]

$$\frac{d^2 I}{d\omega d\Omega} = \frac{e^2}{4\pi^2 c} \left| \int_{-\infty}^{\infty} \frac{\vec{n} \times [(\vec{n}-\vec{\beta})\times\dot{\vec{\beta}}]}{(1 - \vec{\beta} \cdot \vec{n})^2} e^{i\omega(t-\vec{n}\cdot\vec{r}(t)/c)} dt \right|^2 . \tag{10}$$

Here $\vec{\beta}(t) = \vec{v}(t)/c = \dot{\vec{r}}(t)/c$ and $\vec{n}$ signifies the direction of photon emission. When comparison is made to experimental data, an average over populated trajectories should further be included.

Fig. 2 shows a radiation spectrum recorded for positrons moving along the {110} planes in a silicon single crystal[12]. The intensity is normalized to the Bethe-Heitler value obtained for an amorphous target of the same material and thickness, *cf.* Equation (1). A sharp peak, enchanced by a factor of 35 above the amorphous yield appears at approximately 40 MeV, higher harmonics being weak. The solid line shows the result of a theoretical calculation based on the expression (10). Clearly, the agreement between experiment and theory is very satisfactory. In high-energy experiments, the opening angles of photon detectors are usually large compared with $1/\gamma$. Correspondingly, the peak in fig. 2 is sharp only on the high-energy side whereas it falls off smoothly towards low energies. A sharp low-energy cut-off requires collimation to angles small compared with $1/\gamma$. It should be noted that the photon peak is tuneable; a variation of the primary energy in the range 2-10 GeV causes the peak to move from 8 to 70 MeV. So channeling radiation from GeV positrons offers a unique tool as a monoenergetic γ-source in the MeV-region.

4. RADIATION IN THE MULTI-GeV REGION

When the energy of the incident electron or positron is raised further into the region of several tens of GeV, the classical description of the radiation process, e.g., by formulae like

(10), becomes invalid. Clearly, the problem here is not the quantization of the transverse motion of the charged particles since the density of states increases with γ. Instead, the breakdown is associated with the recoil due to the radiation. From simple classical arguments, it is evident that the ratio of the instantaneously emitted power to the primary energy increases with γ. The coherent part of the spectrum extends over an increasing fraction of the available energy $E-mc^2$ ($\approx E$). Correspondingly, a multi-GeV electron (or positron) has a fair chance to emit a photon whose energy amounts to an appreciable fraction of the projectile energy. Such a situation demands a quantum description.

When ultrarelativistic particles ($\gamma \sim 10^5$-10^6) move near axial directions in single crystals the particles "see" enormous strong fields due to the Lorenz contraction of distances between nuclei. Such strong fields are normally described by the parameter $\chi_s = \frac{\gamma E_s}{E_0}$, where E_s is the typical field of the axis and $E_0 = \cdot 10^{16}$ V/cm is the critical field. For $\chi_s << 1$ we are in the classical region and quantum recoil effects can be disregarded. For $\chi_2 \gtrsim 1$a quantum description is needed. Here it should be noted that for $\chi_s = 0.1$ classical calculated radiation intensities are already 1.5 times higher than the correct result.

A full description of the multi-GeV radiation process in terms of quantum electrodynamics has not been given. However, a group of Novosibirsk physicists has developed a very useful semiclassical method which makes effective use of the fact that the projectile motion through the crystal is classical[13, 14]. The method was originally applied to the case of synchrotron radiation emission in very intense fields[15]. Actually, a further simplification applies at these very high impact energies: The range of photon-emission angles relative to the local direction of motion of, for example, an axially channeled electron or positron is small compared with the excursions in projectile angle relative to the axis, $1/\gamma \ll \psi_1 \propto 1/\gamma^{1/2}$. The radiation emitted at two different points adds coherently only when the angle between the two tangents to the (original) particle trajectory is less than the opening angle of the radiation cone. Consequently, the transverse distance traversed by the channeled high-energy projectile during coherent photon emission is small compared with distances over which the continuum potential, or rather its derivative, varies significantly. The emission appears locally as in a constant electromagnetic field, a case treated in great detail in the literature both by means of the semiclassical method[14b] and by more exact methods[16]. With $\eta \equiv \hbar\omega/E$, the photon spectrum for emission in a constant field of magnitude $\mathcal{E} = |\nabla_\perp U|$ reads

$$\frac{dN}{d\eta} = \frac{2\alpha}{\sqrt{3}\lambda}\frac{1}{\gamma}\left[\left(1-\eta+\frac{1}{1-\eta}\right)K_{2/3}(\xi) - \int_\xi^\infty K_{1/3}(t)\,dt\right], \tag{11}$$

$$\xi = \frac{2\eta}{3(1-\eta)\kappa}, \quad \kappa = \mathcal{E}\frac{\lambda}{mc^2}\gamma,$$

where $K_{1/3}$ denotes a modified Bessel function of order $1/3$. To obtain the spectrum observed for, e.g., a channeled particle, it suffices then to make an average of the expression (11) over the field strengths encountered in the crystal by that particle.

In the theory of Baier et al.[13-16] is shown that there exists a characteristic angle θ_0, which discern between strong field effects and perturbative effects (Born approximation). $\theta_0 = \frac{U_0}{mc^2}$, where U_0 denotes the depth (or height) of the potential at the string or planar position. m is the electron rest mass. θ_0 is independent of particle energy and equals for most cases (0.5-1) mrad.

The constant-field approximation, (11), demands that the variations in orientation angle of the projectile be large compared with $1/\gamma$. In the multi-GeV region, this requirement is fulfilled for channeled particles, as described above, as well as for particles incident somewhat beyond the channeling region: The radiation probability is highest in the regions where the field is strongest, which obviously means near the crystal axes and planes. We therefore expect the constant-field result (11) to apply approximately for cases where $\Delta\psi > 1/\gamma$, that is, for incidence angles ψ to a crystal axis or plane fulfilling the inequality

$$\psi < \theta_0 \equiv \frac{U_0}{mc^2}. \tag{12}$$

We then find that, to lowest order, we may use the constant-field approximation (with proper averaging over the particle flux in transverse space) for angles less than θ_0, whereas beyond this angle we may apply the perturbation-limit result, the coherent bremsstrahlung formulaes. First-order corrections for each of the regions $\psi < \theta_0$ and $\psi > \theta_0$ have been given in Reference 14 for the axial case. For the region of small angles, the correction is proportional to the square of the incidence angle, but such that the variation is considerable more rapid for soft photons, $\eta \ll 1$, than for harder ones. For the latter, θ_0 is indeed characteristic for the angular variation, whereas for the former, the result (11) (with first-order correction) cannot be used all way out to θ_0.

II THE PRESENT EXPERIMENTAL SITUATION IN THE MULTI-GeV REGION

The radiation from multi-GeV electrons and positrons traversing thin single crystals has been investigated by two CERN-collaborations: NA42[17] (NA33) and NA43[18] (WA81). The two experiments used the H2-beam in the North Hall, which is ~ ± 30 μrad in divergence. The two experiments differed in the sense that NA42 had no equipment on the incident side to improve the angular resolution, whereas NA43 used driftchambers 50 m apart giving an incident angular resolution of ~ 2 μrad.

Originally NA33 and WA81 found that the radiation intensity from 170 GeV[19] and 150 GeV[20] electrons and positrons was enhanced by factors of 20 and 50 in Ge and Si crystals respectively when incident angles were smaller than θ_0 - the critical angle for strong field effects. For 150 GeV electrons, however[20], an unexpected peak in photon spectra was found.

Surprisingly the intensity of the peak changed drastically by just tilting the crystal 17 μrad even in the H2 beam with divergence of ± 30 μrad.

Soon after, different explanations of the peak were given ranging from: "new" physics to just multiphoton effects[20-25]. In general it is accepted that a well-aligned electron will emit several photons while traversing a few hundred μm thick crystal near an axial direction. All the emitted photons will be added up by the photon detector. Furthermore, it is proposed that the multiple scattering of the incident electrons is counteracted and for some states of motion more that compensated by radiative "cooling" from photon emission. This effect should be strongly influenced by increasing the crystal thickness and electron energy. In very recent papers Kononets and Ryabov[25] show that in the 100-GeV region both multiple scattering and the radiative cooling have a strong influence on the photon peak for incident directions close to axial ones. The multiple scattering causes transitions between random and channeled particles. The radiative cooling increases the probability of hard-photon emission for channeled particles and promotes transitions from random particles to channeled ones, so the multiphoton peak appears only after some thickness of crystal.

Detailed investigations by NA43[26, 27] with the very good angular resolution (2 μrad) has cleared up the problems.

In fig. 3 is shown the photon spectra from 150 GeV electrons incident on <110> Si crystals with thicknesses from 100 μm (a) and up to 1400 μm (d). The statistical uncertainties are within the dot sizes. The aligned spectra are given for different regions of incident angles to the <110> axis. The largest incident angle region was chosen so that the peak structure have just disappeared - this angular region increases with crystal thickness. In fig. 4 is shown the same type of spectra from 200 μm (a), 400 μm (b), and 600 μm (c) thick <110> Ge crystals. Also here statistical uncertainties are within dots but for the highest energies the uncertainties are around two times the dot size. In fig. 5 is shown the energy dependence of photon spectra form the 600 μm <110> Si (fig. 5a-5c). Fig. 5d shows for a comparison the photon spectra from 240 GeV electrons traversing the 400 μm <110> Ge crystal. Only in the last case the statistical error is larger than dot size namely around three times for the high photon energies with lowest statistics.

In all spectra it is seen that the peak structure disappears for incident angle larger than half the Lindhard critical angle ψ_l for channeling. Looking apart from figs. 3a and 5a all spectra can be considered as consisting of two destributions i.e. (1) a broad structureless one as obtained from incident angles larger than - $0.5\psi_l$ and (2) a peaked distribution with a maximum between 0.8-0.9 times particle energy - slightly increasing with particle energy. For the best channeled electrons the content in the peak correspond to more than 20% of the incident particles. The influence of multiple scattering and radiation cooling on the present data cannot be extracted in a simple way but requires comparison with detailed calculations.

In fig. 6 is shown a comparison between the data shown in fig. 3 and some very recent calculations by Kononets and Ryabov[25]. The agreement is very good but only obtained by using the amount of multiple scattering as a fitting parameter. In fig. 7 is shown a comparison with the Ge-data (fig. 4) and calculations by the Baier group[23]. Here the agreement is fair, but the calculated curve for best channeled electrons is lower than the experimental one - an unusual situation.

The multiplicity of the photon emission was also measured by NA43 and is shown in fig. 8. Here is plotted the photon spectrum of fig. 3d parted up in energy slices for which the electron/positron multiplicity was measured in a solid state detector sitting behind a lead converter 5 mm thick (on average - 50% photon conversion). So that 150 GeV well-aligned electrons emit 18-20 photons by traversing a 1.4 mm thick Si crystal.

The strong crystalline fields exert dramatic effects on the energy loss of multi-GeV electrons and positrons. In fig. 9 is shown the radiative energy loss taken from figs. 3 to 5. We see, for example, that in a 0.5 mm Ge crystal 150 GeV/c axially channeled electrons lose more than 50% of the total energy as compared to around 2% in amorphous Ge.

III THE PROPOSED EXTENSION OF NA43

The NA43 results shown above were all for particle incidence close to axial directions (the channeling region). By the end of the run, however, a few investigations were made for incidence around θ_0, where the influence of the strong fields still should be seen. In fig. 10 is shown the surprising results obtained for 150 GeV/c incident on a 200 μm thick <110> W (ab) and a 1.4 mm thick <110> Si (c) crystal. For the W-case it is seen that as the incident angle (given in the figures) to the axis increases beyond 1 mrad (θ_0 = 0.8 mrad) a pronounced high-energy peak appears but the enhancement decreases. The crystal thickness is only 6% of a radiation length so multiple photon emission is small. The more rapid extinction of the soft photon emission than of hard photon emission is an effect predicted by Baier et al.[13-15] for the angular region close to θ_0. For this angular region both the CFA with first order corrections and the first Born CB Scheme become invalid. In fig. c is shown results for incidence around $2\theta_0$ to the {211} plane in Si. A theoretical curve calculated in the Born approximation (full drawn) gives surprisingly a lower yield than the experiment.

Different authors have discussed the use of CB peaks at the highest energy existing or planned. Bilokon et al[28] investigated various aspects of CB at 150 GeV in order to improve the photon beams at the CERN-SPS. Tannenbaum investigated possible uses of CB beams at Fermilab[29] and at the proposed supercollider (SSC)[30]. Fig. 11 shows calculated CB-spectra for 150 GeV (a), 450 GeV (b), and 10 TeV (c). It should be noted that the relative peak energy increases with incident energy. Polarization was found to be between 20% and 55%. Many experiments in particle physics are proposed i.e. photoproduction, searches for toponium, Higgs etc. (for details see ref. 2, 30, and 31). It should be mentioned that the CB spectra (fig. 11) is calculated using the Born approximation and incident angles are usually ~ mrad away from the crystal axis.

The recent experiments on strong field effects have revived this field theoretically - especially by the Baier group[13-16]. Very recent calculations by this group using the complete theory for the interaction of electrons with strong fields or the constant field approximation with corrections have led to very interesting results shown in figs. 12 and 13. Here is shown the results for 150 GeV, 200 GeV, and 250 GeV electrons incident on diamond Si, Ge, and W crystals. The critical angle θ_0 for the four crystals are (following the U_0-values given in ref. 16) C: 0.20 mrad,Si: 0.25 mrad, Ge: 0.40 mrad, and W: 0.80 mrad. The spectra are single photon spectra normalized to the Bethe-Heitler yields and given as a function of photon energy (in units of particle energy). The striking result is that for incident angles around θ_0

dramatic enhancements are expected even for energies around 200 GeV. As compared to the results of Tannenbaum (fig. 10) the enhancements from strong axial fields are 5-10 times higher for the same incident energies.

THE EXPERIMENT

It is proposed to investigate in detail the coherent radiation from Multi-GeV electrons/positrons traversing single crystals of diamond, Si, and Ge. If W will be available with low mosaic spread they will be used as well. These crystals are expected to have very different enhancements (figs. 11 and 12) and the angular dependence of the enhanced effects are also expected to vary (large variation in θ_0). Another aim of the experiment is to find the optimal azimuthal angle for incidence and the crystal thickness giving best enhancement.

Experimental considerations

The beam line

For the investigations is needed an electron/positron beam with energies up to around 200 GeV or more. The angular divergence should be 50 μrad or better. The intensity should be rather low: 10^2-10^5 particles/sec - not to produce pile-up in the solid state detectors. In fig. 14 is shown a layout of the experimental setup used in NA43. A bending magnet is needed to dump the electron beam away from the photon detector positioned in the forward direction. A beam diameter of less than ~ 10 mm is required for our crystal converters and semiconductor detectors.

The requirements are fulfilled by the H2 in the North Hall which was used by some of us in NA43.

The targets.

The targets will be diamond, Si, and Ge (W) single crystals with thicknesses ranging from a few hundred μm up to a few mm. The crystals are first tested for bending and mosaic spread and cut with preferred crystal orientation. The targets are mounted in a highly stabilized channeling goniometer, where cooling to around 90K is possible.

The goniometer is mounted in our channeling vacuum chamber on which high resolution drift chambers are mounted. Alignment and target spots can be controlled on-line by the drift chambers. The detailed scanning is performed by the goniometer.

In order to prevent bending due to cooling, the crystals are fixed at the top with glue in only one point and thereby hanging free. This technique has until now given nearly strain free mountings. The Si and Ge crystals are available commercially without mosaic spread. The much more expensive diamond crystals will be supplied by the Avakian group and the Sellschop-group. The Yerevan group has for more than 10 years used such crystals for CB-production.

Angular resolution

The angular spread of the electron/photon beam is expected smaller than 50 μrad. The goniometer has a step-angle variation of 10 μrad, which should be compared to the characteristic angle for strong field effect θ_0 and the critical angle for channeling $\psi_1 \sim 50$ *μrad*. The values of θ_0 range from 0.2 mrad to 0.6 mrad.

Crystal alignment

The crystals will be aligned by using the well known channeling radiation. The electrons are swept out of the photon beam by the bending magnet bend 3. The photons are detected by an array of lead-glass detectors.

Photon detector

We plan to use lead-glass detectors to detect the total energy of the photons. This calorimeter could also give information about the number of photons by introducing a lead converter and a solid state detector to detect the number of charged particles from photon conversion.

Data-taking and running time

The event structure in the present experiment is very simple and will be written on tape using a small computer. Since optimal crystal thickness have to be found experimentally, the total running time is hard to estimate beforehand. Two weeks of beam-time are the estimated running time including installation and setup.

References

1. Heitler, W. (1954) *The Quantum Theory of Radiation*, Clarendon, Oxford.

2. Diambrini Palazzi, G. *Rev. Mod. Phys.* **40** (1968) 611.

3. Ter-Mikaelian, M.L. (1972) *High-Energy Electromagnetic Processes in Condensed Media*, Wiley, New York.

4. D.S. Gemmell, Rev.Mod.Phys. 46 (1974) 129.

5. E. Uggerhøj, Phys.Scripta 28 (1983) 331.

6. A.H. Sørensen and E. Uggerhøj, Nature 325 (1987) 311.
   A.H. Sørensen and E. Uggerhøj, Nucl. Science Appl. Vol. 3 (1989) 147.

7. V.V. Beloshitsky and F.F. Komarov, Phys.Rep. 93 (1982) 117.

8. J.U. Andersen, E. Bonderup and R.H. Pantell, Ann.Rev.Nucl.Part.Sci. 33 (1983) 153.

9. A.W. Sáenz and H. Uberall, *Coherent Radiation Sources*, Springer Verlag, Heidelberg, 1985.

10. Lindhard, J., Kgl. Danske Videnskab. Selskab, *Mat. Fys. Medd.* **34** No. 14; (1964).
    Lervig, P., Lindhard, J. and Nielsen, V. *Nucl. Phys. A* **96** (1967) 481.

11. Jackson, J.D. (1975) *Classical Electrodynamics*, Wiley, New York.

12. Bak, J.F., Ellison, J.A., Marsh, B., Meyer, F.E., Pedersen, O., Petersen, J.B.B., Uggerhøj, E., Østergaard, K., Møller, S.P., Sørensen, A.H. and Suffert, M. *Nucl. Phys. B* **254** (1985) 491.

13. Baier, V.N., Katkov, V.M. and Strakhovenko, V.M. *Nucl. Instrum. Methods B* **16** (1986) page 5.

14. a) Baier, V.N., Katkov, V.M. and Strakhovenko, V.M. *Phys. Lett. A* **117 (1986)** 251.
    b) Berestetskii, V.B., Lifschitz, E.M. and Pitaeskii, L.P. (1971) *Relativistic Quantum Theory*, Pergamon, Oxford (vol. 4 of Landau, L.D. and Lifschitz, E.M., Course of Theoretical Physics).

15. Baier V.N. and Katkov, V.M. Sov. Phys. JETP *26* (1968) 854.

16. Baier V.N., Katkov, V.M. and Strakhovenko, V.M., Nucl. Science Appl. Vol. 3 (1989) 245.

17. NA42: **Study of Unexplained Hard Photon Production by Electrons Channelled in a Crystal**

Albany SUNY, Annecy LAPP, Lyon IPNL

Albany SUNY
Cue, N. - Kimball, J.C. - Marsh, B.B.

Annecy LAPP
Bologna, G - Gouanere, M - Peigneux, J.P. - Sillou, D. - Spighel, M.

Lyon IPNL
Artru, X. - Belkacem, A. - Chevallier, M. - Gaillard, M.J. - Genre, R. - Kirsch, R. - Poizat, J.C. - Remillieux, J.

Spokesman: Remillieux, J. Contactmand: Spighel, M.

18. NA43: **Investigations of the Energy and Angular Dependence of Ultrashort Radiation Lengths in Si, Ge and W Single Crystals**

Aarhus Univ., CERN, Strasbourg CRN/ULP, Stuttgart MPI f. Metallf.

Aarhus Univ.
Medenwaldt, R. - Møller, S.P. - Petersen, J.B.B. - Sørensen, A.H. - Tang-Petersen, S. - Uggerhøj, E.

CERN
Elsener, K.

Strasbourg CRN/ULP
Heitz, C. - Siffert, P. - Stoquert, J.

Stuttgart MPI f. Metallf.
Maier, K.

Spokesman; Uggerhøj, E. Contactman: Elsener, K.

19. J.F. Bak et al., Phys. Lett. B 213 (1988) 242.

20. A. Belkacem et al., Phys. Rev. Lett. 54 (1985) 2667, A. Bekacem et al., Phys. lett. B 177 (1986) 211.

21. V.V. Tikhomirov, Phys. Lett. A 125 (1987) 411; Nucl. Instrum. Methods B 36 (1989) 282.

22. X. Artru, Phys. Lett. A 128 (1988) 302.

23. V.N. Baier, V.M. Katkov and V.M. Strakhovenko, Phys. Lett. A 132 (1988) 211.

24. Y.V. Kononets and V.A. Ryabov, Pis'ma Zh. Eksp. Teor. Fiz. 48 (1988) 303 [JETP Lett. 48 (1988) 333].

25. Y.V. Kononets and V.A. Ryabov, in: Proc. ICACS-13, Nucl. Instrum. Methods B 148 (199) 269, 274.

26. R. Medenwaldt, S.P. Møller, A.H. Sørensen, S. Tang-Petersen, E. Uggerhøj, K. Elsener, M. Hage-Ali, P. Siffert, J. Stoquert., and K. Maier, Phys. Rev. Lett. 63 (1989) 2827.

27. R. Medenwaldt, S.P. Møller, A.H. Sørensen, S. Tang-Petersen, E. Uggerhøj, K. Elsener, M. Hage-Ali, P. Siffert, J. Stoquert, P. Sona, and K. Maier, Phys. Lett. B 242 (1990) 517.

28. H. Bilokon et al., Nucl. Instr. & Meth. 204 (1983) 299.

29. M.J. Tannenbaum, 1980 Symposium on high energy physics with polarized beams and polarized targets. Lausanne, Switzerland, Sept. 1980 (BNL report 28586).

30. M.J. Tannenbaum, SSC Fixed target workshop, The Woodlands, Texas, January, 1984 (BNL report 34614).

31. A. Schäfer, S. Graf, J. Augustin, W. Greiner, and E. Uggerhøj, J. Phys. G., Nucl. Part. Phys. 16 (1990) L 131.

Figure Captions

Fig. 1. Coherent bremsstrahlung as obtained in the Born approximation for 10 GeV electrons or positrons incident at an angle of 1 mrad to the <110> axis of a germanium single crystal kept at room temperature. The displayed spectra are power-spectra. In a) the beam is incident parallel to the {110} plane whereas in b) a "random" value of the azimuthal angle is chosen (0.3 rad relative to the {110} plane). Dashed curves represent the Bethe-Heitler yield.

Fig. 2. Channeling radiation by 6.7 GeV positrons incident parallel to the {110} plane in a 0.1-mm thick silicon single crystal kept at room temperature. The intensity is normalized to the incoherent bremsstrahlung yield that pertains to an amorphous target of the same material and thickness. The solid curve represents theoretical values.

Fig. 3. Enhancements, relative to random, of gamma radiation for 150 GeV e^- incident on (a) 100 μm, (b) 165 μm, (c) 600 μm, and (d) 1400 μm thick <110> Si crystals. The incident angle regions to the <110> axis are given in μrad. Photon energies are in units of the particle energy E_0.

Fig. 4. As in fig. 3 but targets were a) 200 μm, b) 400 μm, c) 600 μm thick <110> Ge crystals.

Fig. 5. Same type of spectra as fig. 3, but for varying particle energy E_0: (a) 70 GeV e^- incident on 600 μm <110> Si, (b) 150 GeV on 600 μm Si, (c) 240 GeV e^- on 600 μm <110> Si, (d) 240 GeV e^- on 400 μm <110> Ge.

Fig. 6. Comparison between the experimental results of fig. 3 and calculations by Y.V. Kononets and V.A. Ryabov[25].

Fig. 7. Comparison between the experimental results of fig. 4 and calculations by the Baier-group[14].

Fig. 8. Electron/positron multiplicity for the photon spectrum from 150 GeV/c electrons traversing 1.4 mm <110> Si-crystal (fig. 3d).

Fig. 9. Radiative energy loss for electrons incident on <110> Si and Ge crystals of varying thickness given in mm. The incident angle region was (0-7) μrad to the <110> axis. The dashed curves correspond to the largest incident angle regions of present data (fig. 3-5). The particle energies are given in the figure. The value for the W-crystal is shown also.

Fig. 10. Photon spectra from 150 GeV/c electrons incident on a 200 μm <110> W at 1 mrad (a), 2 mrad (b) and 4.5 mrad (c) to the axis. (d) photon spectrum from the {211} plane for an incidence around 2 θ_0.

Fig. 11. Calculated CB spectrum[29] from diamond and silicon targets at (a) 150 GeV and (b) 450 GeV for possible use at FNAL.

(c) calculated CB spectrum[30] for diamond target at 10 TeV, for possible use at SSC. Note that first Born approximation (used here) may not be applicable at these high energies.

Fig. 12. Calculated single photon spectra for diamond and W: Baier et al.[13-16].

Fig. 13. Calculated single photon spectra fo Ge, Si, and W.: Baier et al.[13-16].

Fig. 14. Experimental setup as used by NA43 in the H2 beam in the North Hall. The inserts show the measured beam divergence in vertical and horizontal directions.

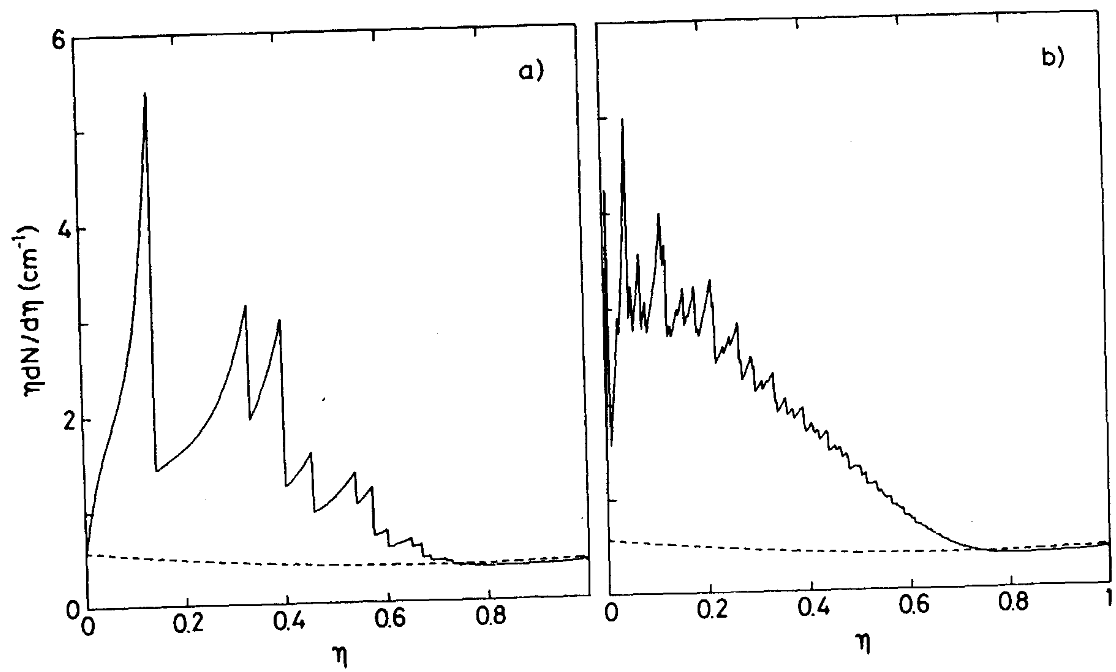

Fig. 1

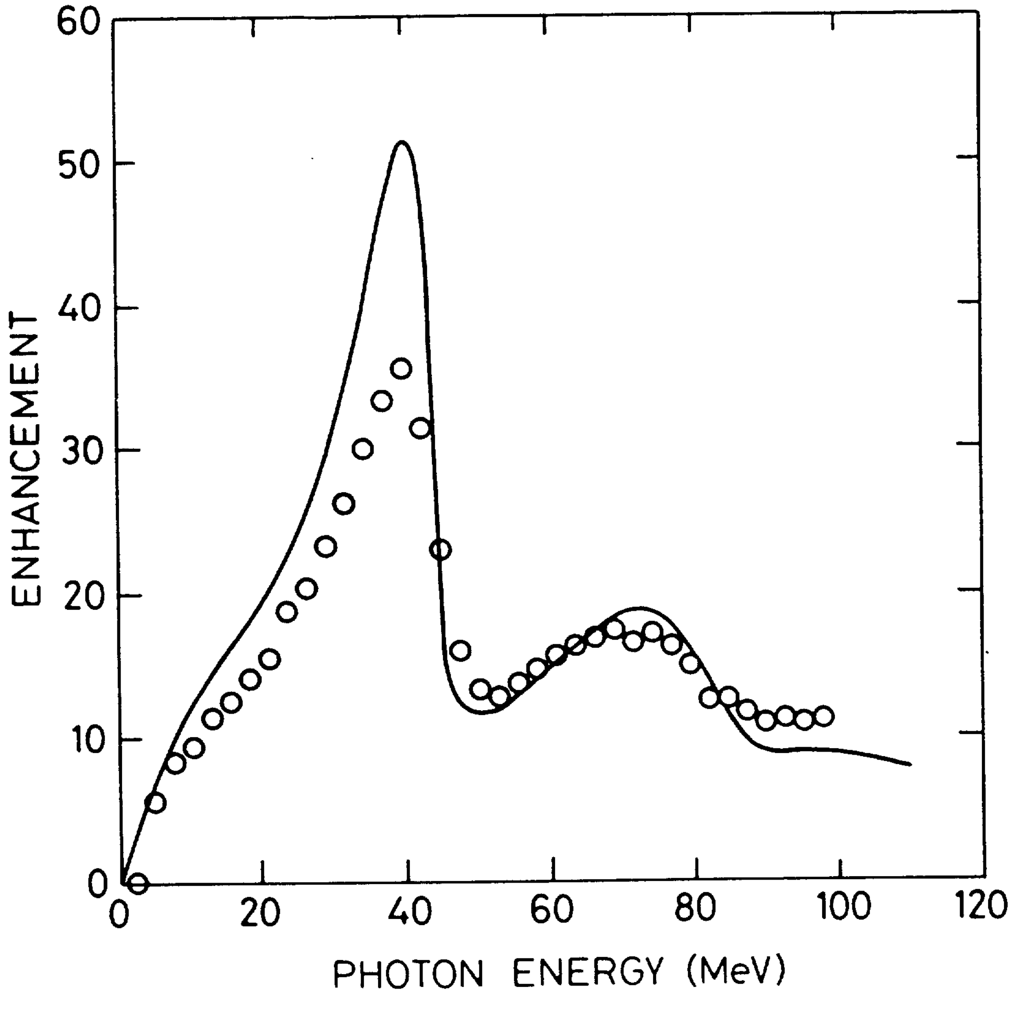
60
50
40
30
20
10
0
ENHANCEMENT
0
20
40
60
80
100
120
PHOTON ENERGY (MeV)

Fig. 2

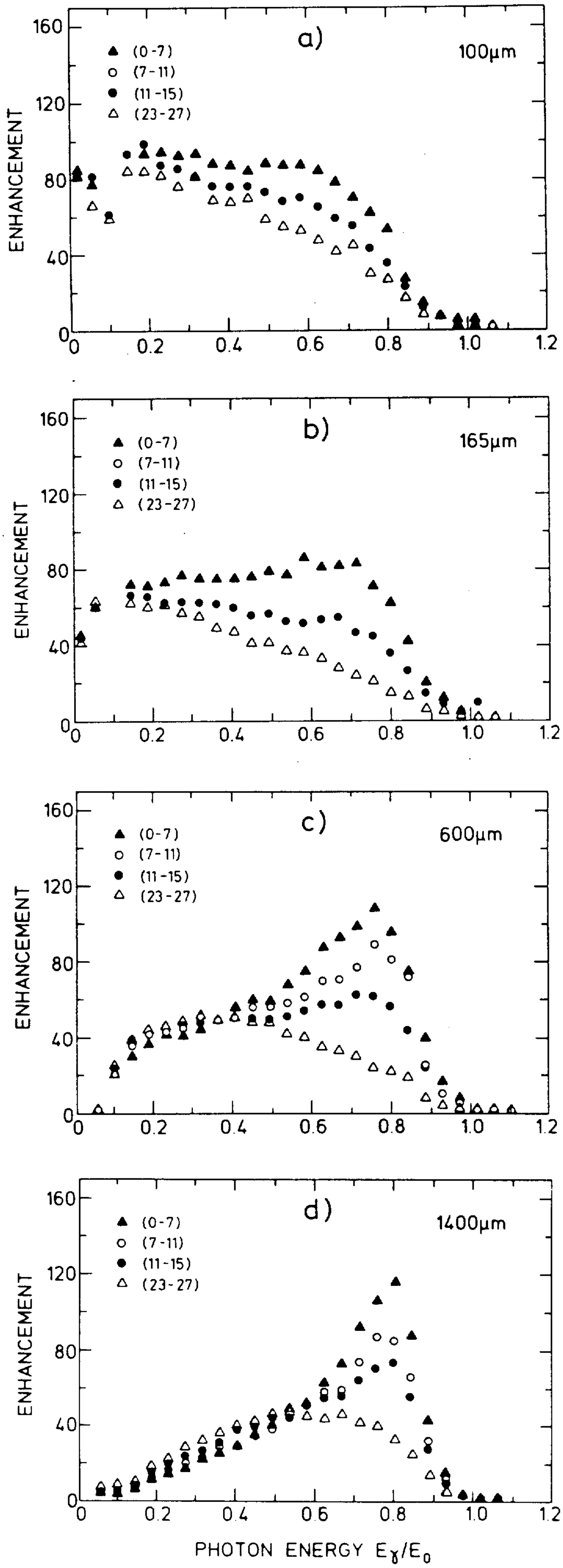
a)
100μm
b)
165μm
c)
600μm
d)
1400μm
(0-7)
(7-11)
(11-15)
(23-27)
ENHANCEMENT
PHOTON ENERGY E_γ/E_0

Fig. 3

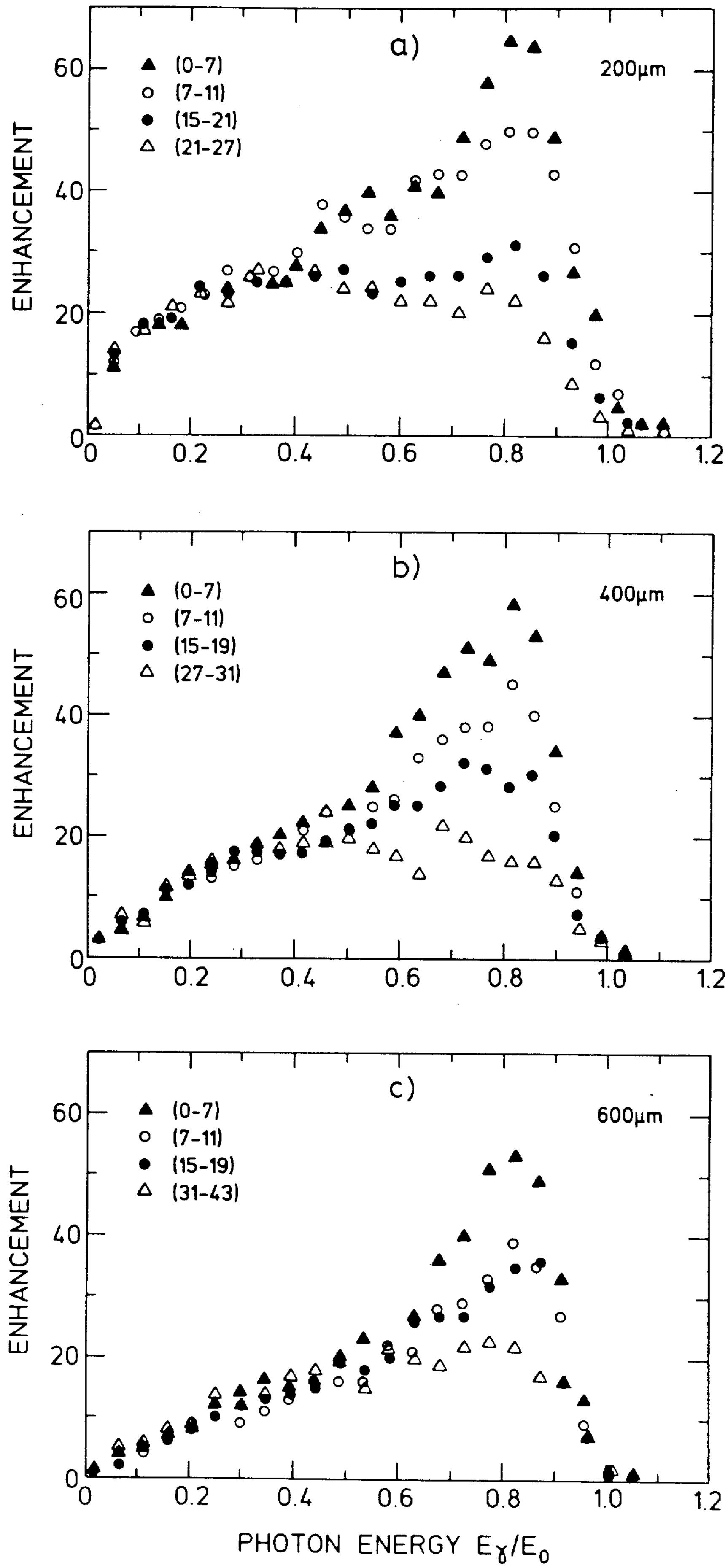
a)
200µm
(0-7)
(7-11)
(15-21)
(21-27)
b)
400µm
(0-7)
(7-11)
(15-19)
(27-31)
c)
600µm
(0-7)
(7-11)
(15-19)
(31-43)
ENHANCEMENT
PHOTON ENERGY E_γ/E_0

Fig. 4

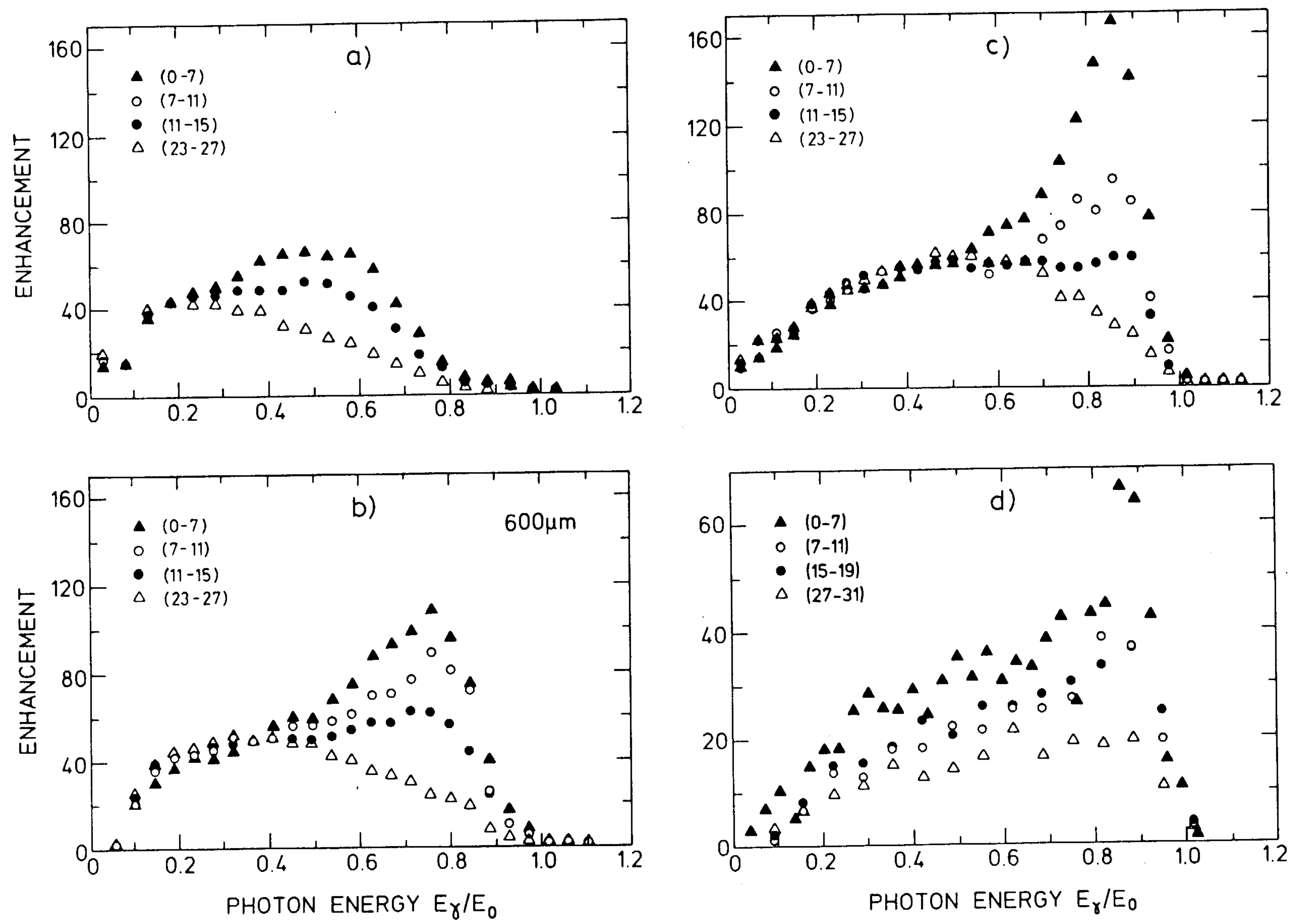
a)
(0-7)
(7-11)
(11-15)
(23-27)
b)
600µm
(0-7)
(7-11)
(11-15)
(23-27)
c)
(0-7)
(7-11)
(11-15)
(23-27)
d)
(0-7)
(7-11)
(15-19)
(27-31)
ENHANCEMENT
PHOTON ENERGY E_γ/E_0

Fig. 5

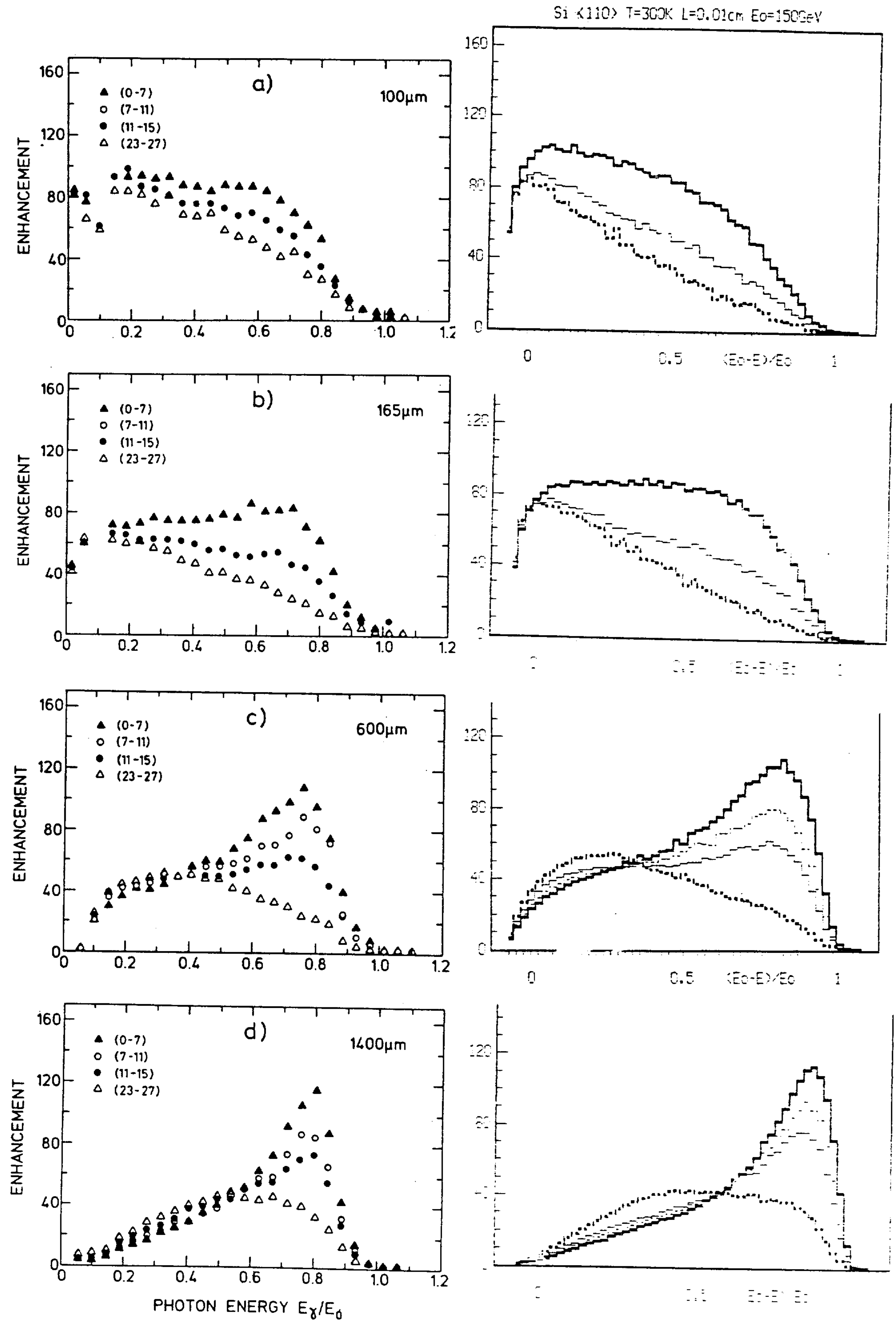
Si <110> T=300K L=0.01cm Eo=150GeV
a)
100μm
b)
165μm
c)
600μm
d)
1400μm
(0-7)
(7-11)
(11-15)
(23-27)
ENHANCEMENT
PHOTON ENERGY Eγ/E0
(Eo-E)/Eo

Fig. 6

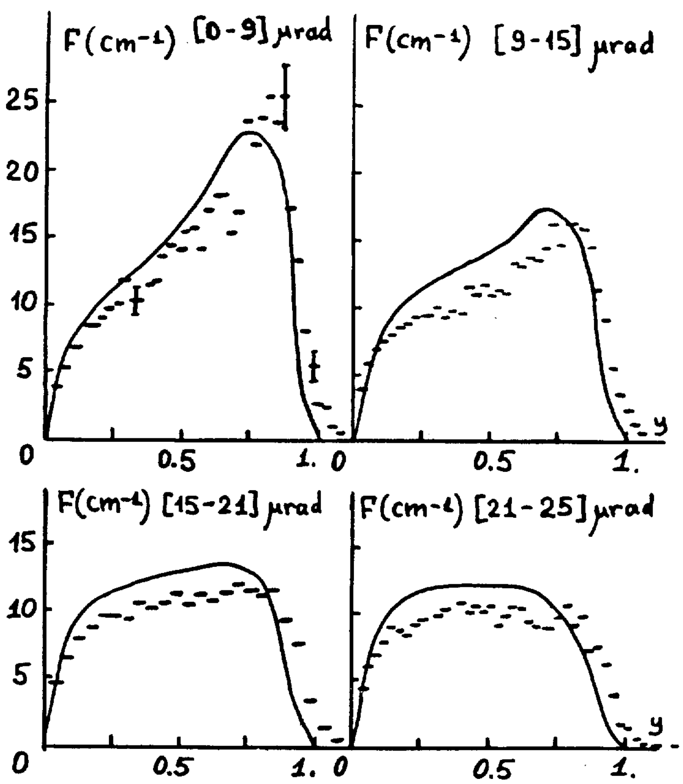

F(cm⁻¹) [0-9] μrad
F(cm⁻¹) [9-15] μrad
F(cm⁻¹) [15-21] μrad
F(cm⁻¹) [21-25] μrad
25
20
15
10
5
0
0.5
1.
y

Fig. 7

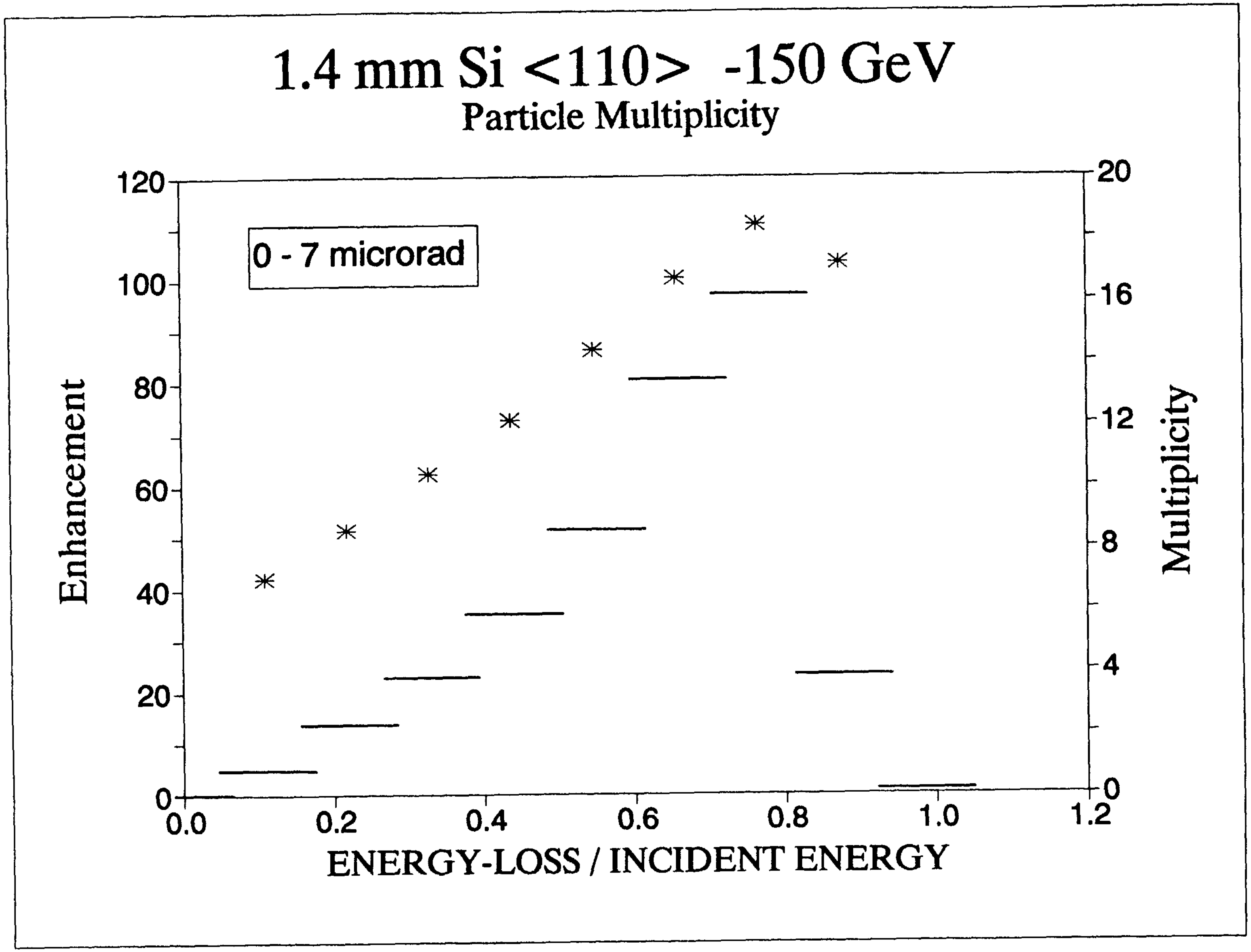
1.4 mm Si <110> -150 GeV
Particle Multiplicity
0 - 7 microrad
Enhancement
Multiplicity
ENERGY-LOSS / INCIDENT ENERGY
0
20
40
60
80
100
120
0.0
0.2
0.4
0.6
0.8
1.0
1.2
4
8
12
16
20

Fig. 8

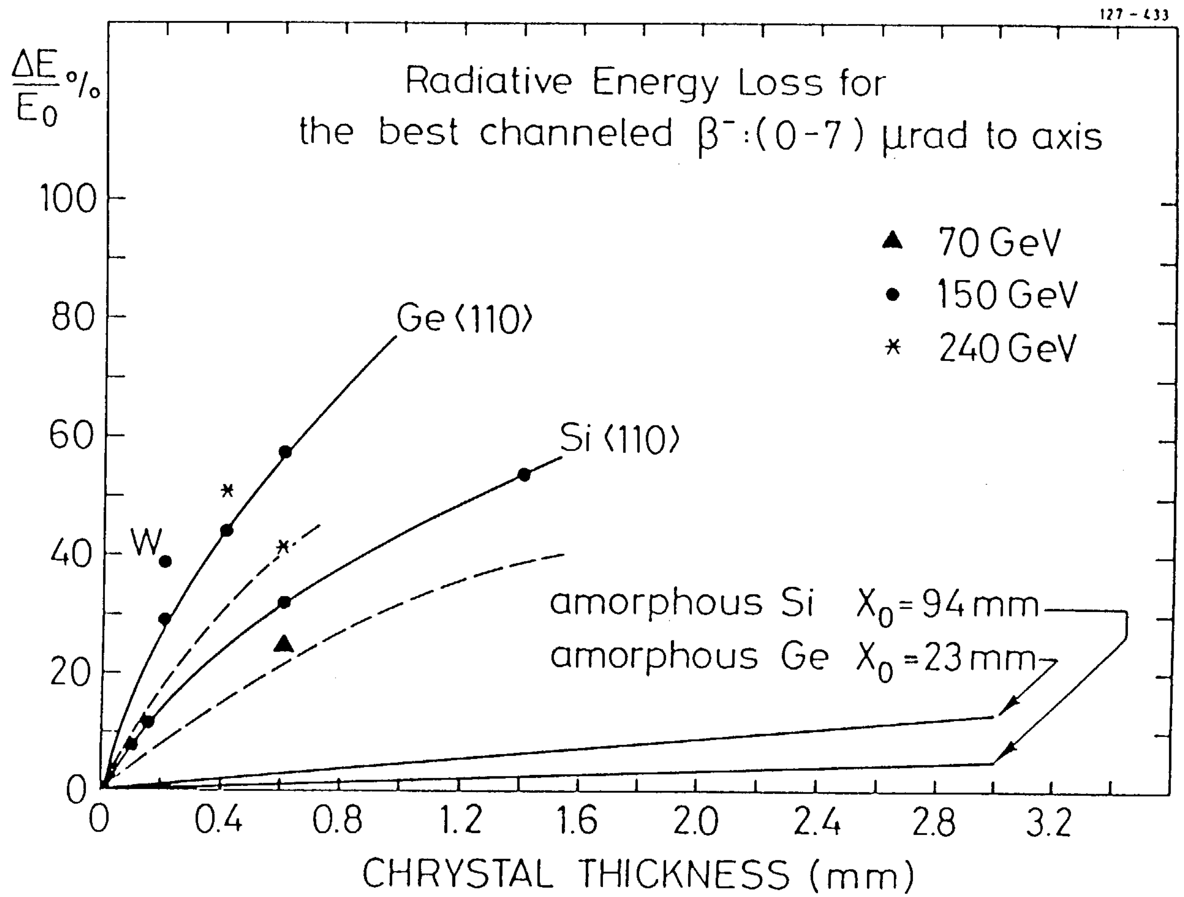
127 - 433
ΔE/E0 %
Radiative Energy Loss for
the best channeled β⁻:(0-7) μrad to axis
70 GeV
150 GeV
240 GeV
Ge ⟨110⟩
Si ⟨110⟩
W
amorphous Si X0 = 94 mm
amorphous Ge X0 = 23 mm
0
20
40
60
80
100
0.4
0.8
1.2
1.6
2.0
2.4
2.8
3.2
CHRYSTAL THICKNESS (mm)

Fig. 9

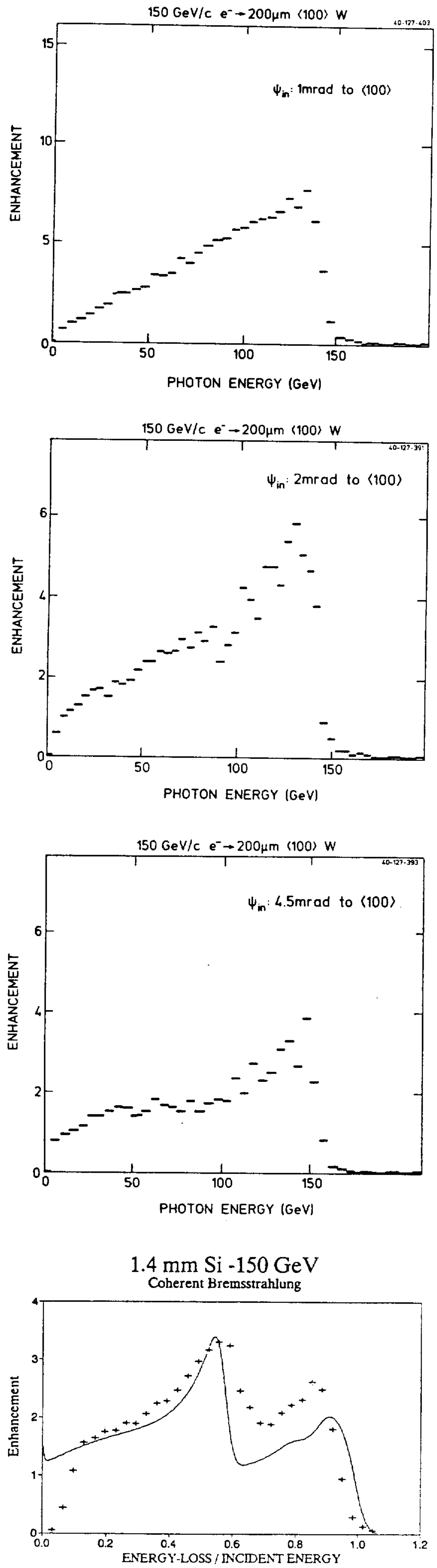
150 GeV/c e⁻→200μm ⟨100⟩ W
ψin: 1mrad to ⟨100⟩
ENHANCEMENT
PHOTON ENERGY (GeV)
150 GeV/c e⁻→200μm ⟨100⟩ W
ψin: 2mrad to ⟨100⟩
ENHANCEMENT
PHOTON ENERGY (GeV)
150 GeV/c e⁻→200μm ⟨100⟩ W
ψin: 4.5mrad to ⟨100⟩
ENHANCEMENT
PHOTON ENERGY (GeV)
1.4 mm Si -150 GeV
Coherent Bremsstrahlung
Enhancement
ENERGY-LOSS / INCIDENT ENERGY

Fig. 10

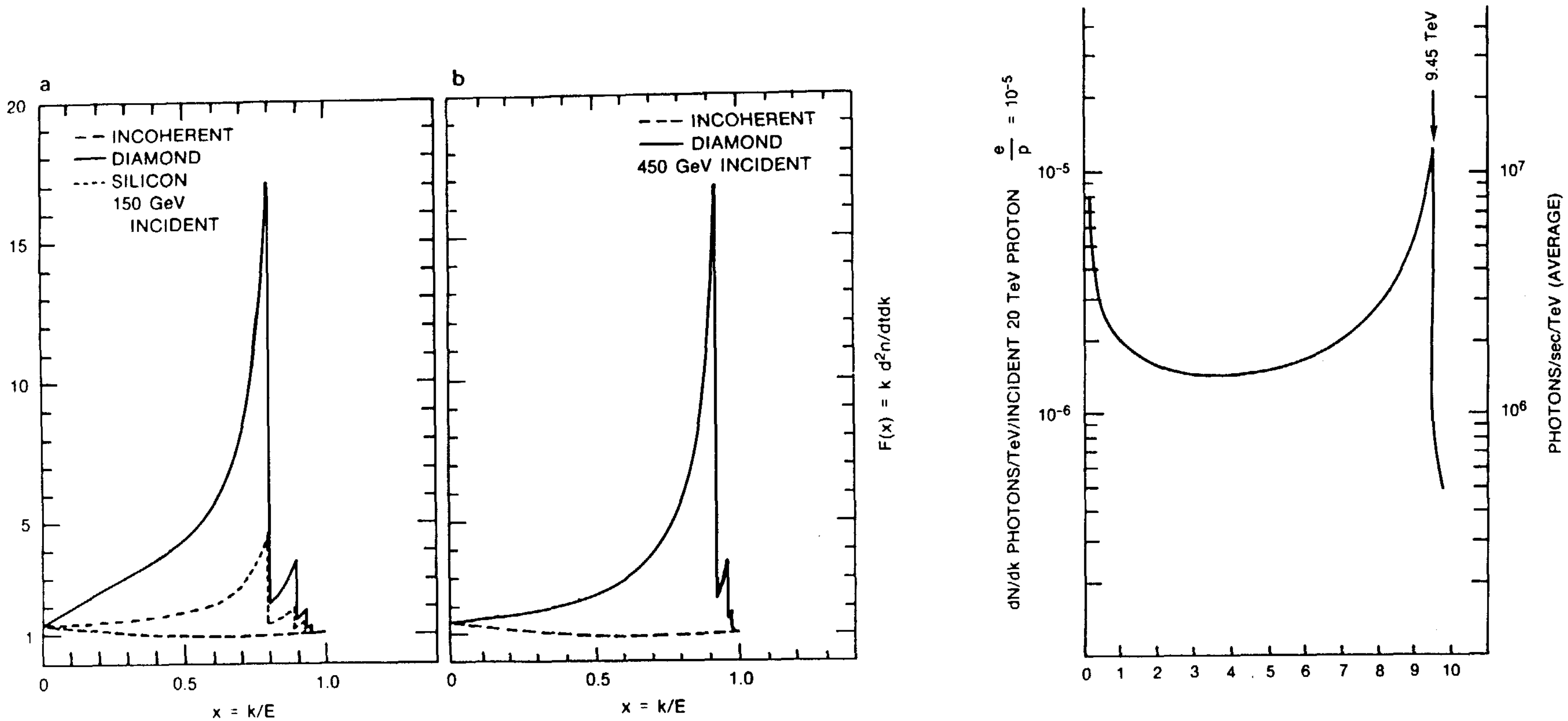
a
b
INCOHERENT
DIAMOND
SILICON
150 GeV
INCIDENT
INCOHERENT
DIAMOND
450 GeV INCIDENT
x = k/E
F(x) = k d²n/dtdk
dN/dk PHOTONS/TeV/INCIDENT 20 TeV PROTON
e/p = 10⁻⁵
9.45 TeV
PHOTONS/sec/TeV (AVERAGE)

Fig. 11

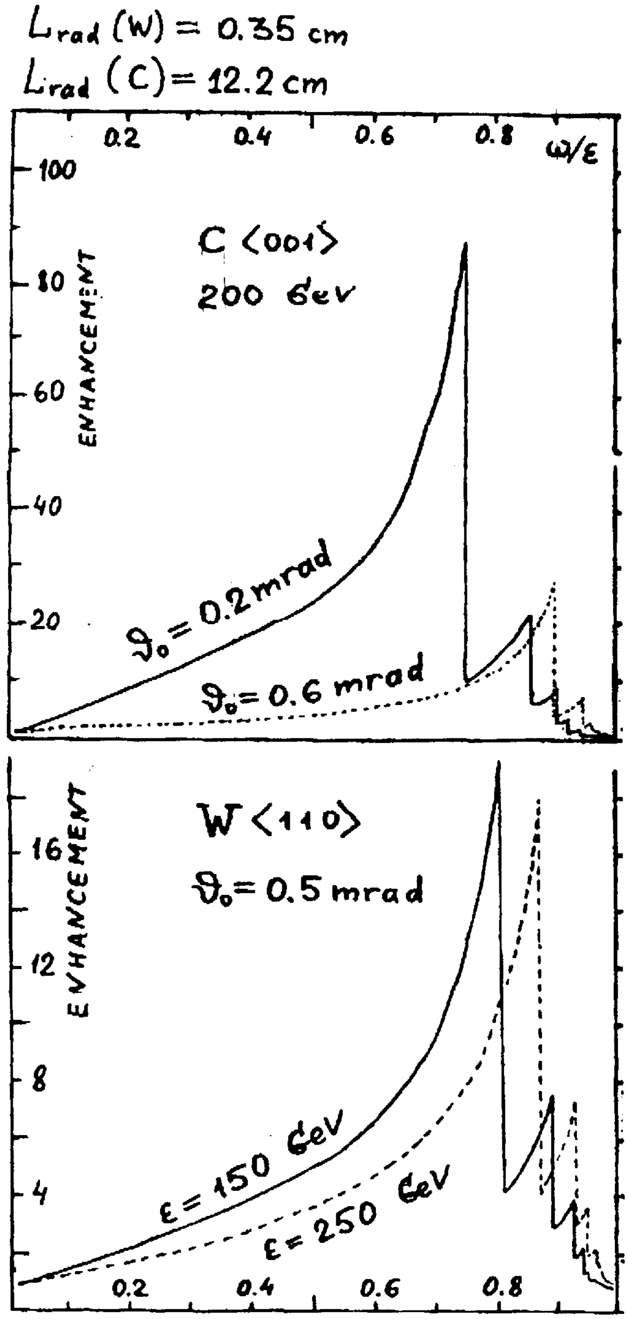

Lrad (W) = 0.35 cm
Lrad (C) = 12.2 cm
0.2
0.4
0.6
0.8
ω/ε
100
80
60
40
20
ENHANCEMENT
C <001>
200 GeV
ϑ₀ = 0.2 mrad
ϑ₀ = 0.6 mrad
W <110>
ϑ₀ = 0.5 mrad
16
12
8
4
ENHANCEMENT
ε = 150 GeV
ε = 250 GeV
0.2
0.4
0.6
0.8

Fig. 12

$L_{rad}(Ge) = 2.3$ cm

$L_{rad}(Si) = 9.4$ cm

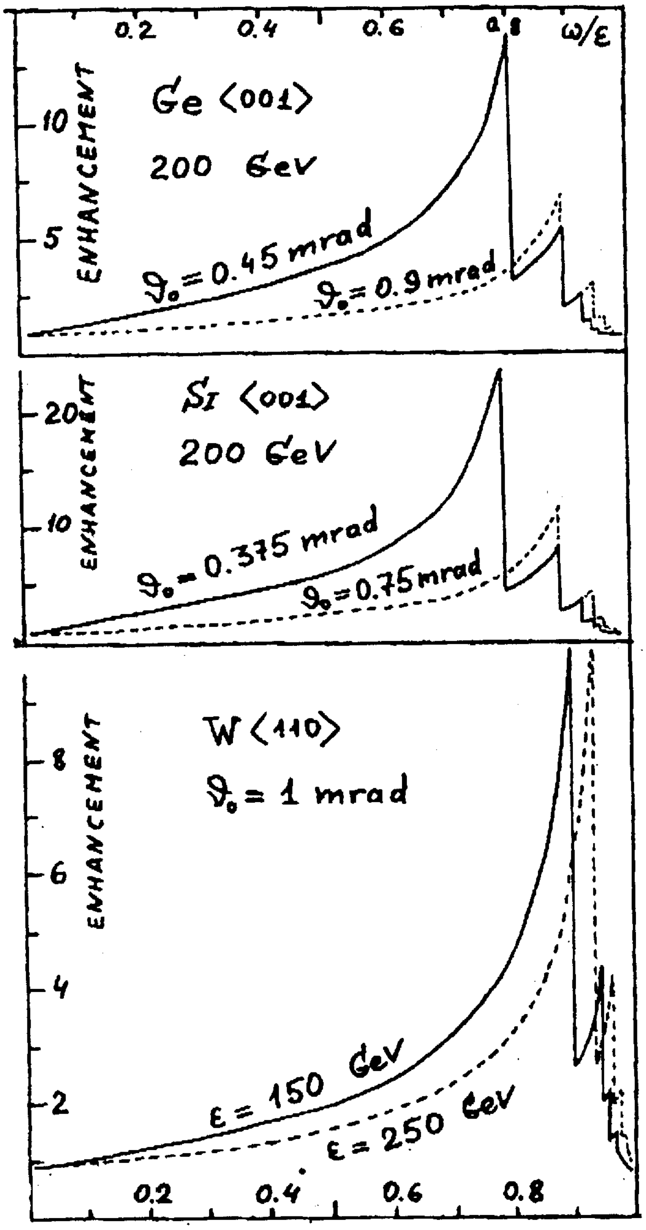

Fig. 13

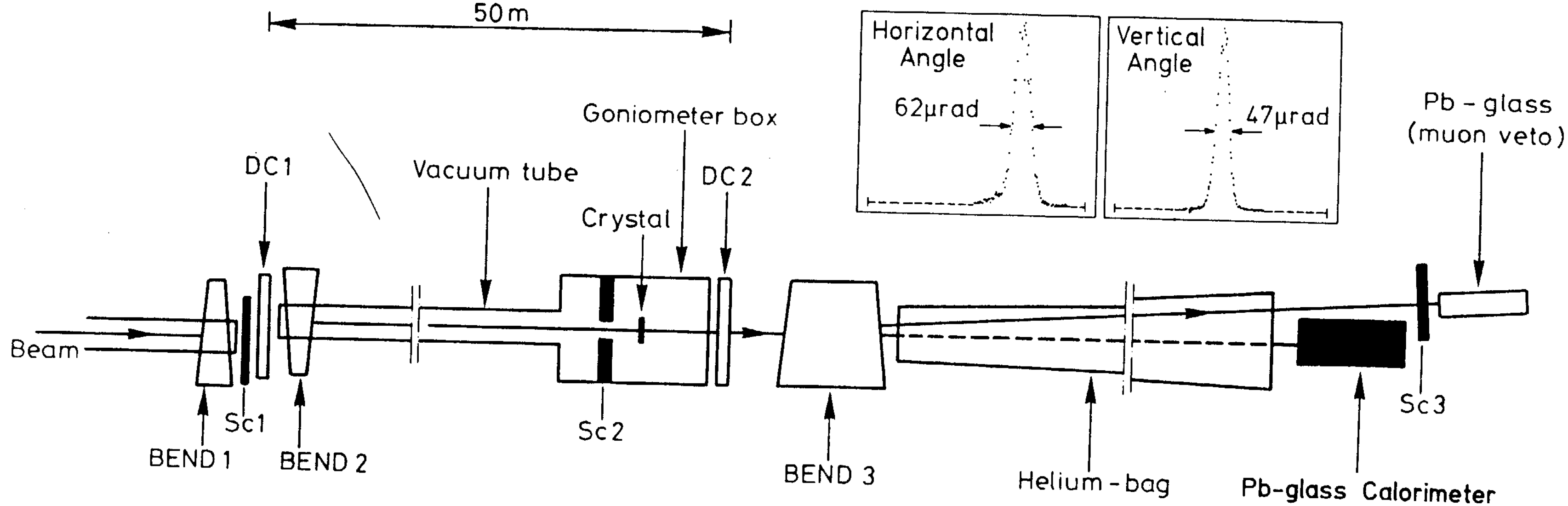

Fig. 14

Imprimé au CERN. Prix : 1.60 Fr.